Na^+ and Cl^- Transport Across Polyimide Films

A. SCHUSSLER,[1] F. BELLUCCI,[1] S. D. SENTURIA,[2] and R. M. LATANISION[1,*]

[1]The H.H. Uhligh Corrosion Laboratory and [2]Microsystems Technology Laboratories, Massachusetts Institute of Technology, Cambridge, Massachusetts 02139

SYNOPSIS

Na^+ and Cl^- transport across 2.4- and 5.2-μm-thick polyimide (PI) PMDA/ODA and 7.5-μm-thick du Pont Kapton films was studied in a diffusion cell using ion-selective electrodes. The temperature was 30°C. Diffusion coefficients D_m (in cm^2/s), permeability coefficients P (in cm^2/s), and distribution coefficients K were obtained by applying the time lag analysis on the ion uptake transient in the acceptor compartment of the diffusion cell. Both Na^+ and Cl^- were observed to diffuse across PI. Diffusion coefficients varied in the range 10^{-12}–10^{-13} cm^2/s whereas ionic permeability results showed more scatter ranging from 1×10^{-11} to 8×10^{-14} cm^2/s. The latter discrepancy was ascribed to diffuse heterogeneities on the order of 0.5 μm. No significant ionic selectivity between Na^+ and Cl^- was observed. This result indicates the absence of ionic fixed charge (unreacted polyamic acid) in the polymeric matrix. An attempt is made to determine the effect of water sorption mode and contaminants in the film on the ionic permeabilities data.

INTRODUCTION

It is recognized that technological advances in areas such as data acquisition, information processing, and communications are dependent on the development of new materials and device structures as well as on their application in microelectronics and other advanced component systems. Considering the trend toward device densification and decreased component size in integrated circuit technology, for example, in addition to the increasingly aggressive service environments in which computer control is being applied, corrosion of electronic materials and device reliability have become important issues. Preventing corrosion phenomena that affect new materials (or new combinations of materials) in electronics is fundamental to successful operation of such advanced systems.

Corrosion phenomena related to interactions among materials and local environments as well as to variations in the operating ambient and contaminants present in the materials themselves, or arising from manufacture, tremendously affect reliability. In essence, corrosion reduces reliability by (i) degrading the structure, (ii) introducing undesirable products, and (iii) reducing performance. In microelectronics, for example, the presence of moisture and other contaminants may lead to chemical attack of the chip metallization or can alter the electrical characteristics of the device.[1]

Currently, corrosion problems affecting reliability are overcome by the use of suitable organic coatings or, in extreme cases, with hermetic ceramic packages, with a general increase in cost and, often, without full understanding of the basic phenomena involved. Most often, packaging materials are chosen for ease of processing with less attention being given to specific aspects of their protectiveness. This approach is typical of the packaging of integrated circuits. In these circuits, packaging costs vary from 15 to 50% of the final cost of the chip.[2]

Corrosion and corrosion-related problems affecting thin films and related geometries involving electronic materials are unique due to the physical scales involved in many of these systems.[3–5] In many cases, dimensions are measured in micrometers and fractions of micrometers for both conductors and dielectrics (coatings). One consequence is that the

* To whom all correspondence should be addressed.

Journal of Applied Polymer Science, Vol. 42, 1567–1577 (1991)
 CCC 0021-8995/91/061567-11$04.00

amount of corrosion that can be tolerated is correspondingly small, particularly in the case of localized corrosion.

For corrosion to occur, certain requirements must be met. First, moisture must be present; this is the electrolyte that provides a medium for ionic transport and is related to the relative humidity and temperature. Second, a supply of cathodic reactant is necessary. This is usually oxygen, and the cathodic process is that of oxygen reduction.

In addition to these basic requirements, the presence of ionic contaminants can significantly increase the rate at which corrosion occurs. Contaminants can be derived from the atmosphere or from the processing of the devices themselves. Examples of contaminants from the atmosphere are chloride ions from airborne sodium chloride and sulfuric acid derived from sulfur dioxide emissions. Other ions, such as sodium, lithium, and chloride ions, can be incorporated into a device during synthesis of the packaging materials or subsequent processing.

Although transport properties for gases and water vapor through polyimide (PI) were described in recent literature,[6-12] little work has been reported concerning ionic transport across PI, despite the increasing use of microprocessors and other hardware in corrosive environments, such as the automobile, chemical, and pulp industries. Sodium transport from or through PI to SiO_2 can also affect device thresholds and create reliability problems.[13] Sodium across PI has been studied under dry conditions,[13] while the only permeability data in the aqueous phase are those describing hydrogen fluoride transport.[14] The high permeability reported in the literature has been explained by the diffusion of the associated species, HF, rather than due to the ionic components H^+ and F^-.[14] In addition, no permeability of PI to HCl, NaOH, and KOH at 5*M* ionic concentration in the feed compartment of the permeation cell was detected in diffusion experiments lasting 20 min or more.[14] As will be shown, 20 min is not sufficient to observe any significant diffusive transport if very low diffusion coefficients ($\approx 10^{-12}$–10^{-13} cm^2/s) are present. This is true even if a membrane as thin as 1 μm is considered.

In this article, ionic (Na^+ and Cl^-) diffusion and permeability data were reported for 2.4- and 5.2-μm-thick PI (PMDA/ODA) and 30 HN (7.5-μm) du Pont Kapton films. Experimental data described in this work were obtained using the PI as a membrane separating two sides of a diffusion cell. Time lag analysis was used to obtain both diffusion and permeability coefficients.

EXPERIMENTAL

Reagents

Polyamic acid was supplied by E.I. du Pont de Nemours and Company as the amic acid solution of poly-[*N*,*N*'-(*p*,*p*'-oxydiphenylene) pyromellitimide].

Samples for ion permeation were in the form of a 4-cm^2 free-standing membrane of film supported by a 2-in. silicon wafer. These membranes were fabricated using standard micromachining techniques.[15] First, a 5-μm-thick square diaphragm of silicon was etched in a (100) silicon wafer from the back using a silicon dioxide etch mask, a 5-μm p^+ diffusion of boron as an etch stop, and 50% hydrazine in water as the anisotropic etchant. The silicon dioxide etch mask was then stripped using hydrofluoric acid. The polymer film of interest was deposited on the wafer using spin coating techniques (6000 rpm for 90 s) and then cured. Two separate PI layers of approximately 1.2 μm thick were used to minimize pinholes. In some samples 4 PI layers were used. A β-stage cure (135°C for 10 min in air) was carried out after applying each layer. The final curing step was performed at 400°C for 45 min in nitrogen. This process was followed by a backside SF_6 plasma etch in order to remove the 5-μm silicon diaphragm. Thus, a suspended membrane of PI was formed.

Kapton 30 HN (7.5-μm thick) was furnished by du Pont Electronic Department, Wilmington, DE. Sodium chloride solutions were prepared from reagent-grade material and dissolved in distilled water (18 MΩ cm resistivity).

Apparatus

Ionic transport through polyimide membranes was investigated using a two-compartment (feed 1 and acceptor 2) quartz permeation cell similar to that recently described.[14] Each compartment of the cell (120 cm^3) was equipped with a magnetic stirrer and heating mats. A temperature controller allowed adjustment of the solution temperature from room temperature to approximately 60°C. However, 30°C was used in all the experiments described in what follows. Additional ports in both half cells allowed insertion of gas bubblers or platinum electrodes. The PI membranes were mounted in the sample holder and sealed with Viton O-rings. A highly concentrated NaCl solution (0.5–5*M*) was placed in the left part of the cell (feed compartment). The right part of the cell contained distilled water (acceptor compartment). Na^+ and Cl^- fluxes through the

membrane were determined by measuring the ion concentration in the acceptor compartment as a function of time. This measurement was achieved by recording the change in potential of an ion-selective electrode relative to a fixed-reference electrode as described in the following sections.

Cl^- Ion Measurement

A Cl^- electrode (Orion, model 94-17B) in combination with a double-junction reference electrode (Orion, model 90-02) was used to determine the Cl^- concentration. The electrodes were placed in the acceptor compartment of the permeation cell, and the potential was recorded with a high-impedance multimeter (Keithley, model 617). Continuous stirring of the solution was required during the measurement procedure. The time response of the electrode (that is, the time required to reach a stable potential reading) ranges from a few seconds in concentrated solutions up to 3 min close to the detection limit, which is approximately 0.04 ppm. No ionic strength adjustor (ISA) was added to the solution since no differences were observed between calibration curves obtained with and without ISA. Although the Cl^- electrode does not exhibit a large potential drift (not more than 2 mV/day), measurements were carried out discontinuously in order to avoid prolonged exposure to very low concentrations.

Na^+ Ion Measurement

A Ross sodium ion combination electrode (Orion, model 86-11) was used to determine the Na^+ ion concentration. The detection limit was found to be approximately 0.02 ppm. Continuous stirring of the solution during the measurement was also required. Because the Na^+ ion-selective electrode is a glass electrode while the Cl^- ion electrode is a solid-state electrode, some differences in the measurement procedure arise:

(i) Before the determination of Na^+, an ISA (1 mL of $4M$ NH_4OH + $4M$ NH_4Cl) was added to the acceptor compartment in order to adjust the pH as well as keep the ionic strength constant. Due to ISA addition, simultaneous measurements of both Cl^- and Na^+ transport were not carried out.

(ii) The time response of the electrode is low compared to the Cl^- electrode. Achieving steady state close to the detection limit required measuring times up to 20 min.

(iii) At low Na^+ ion concentrations a potential drift (about 1 mV/h) occurs during continuous exposure of the electrode due to the replacement of the sodium ion on the glass membrane surface by hydrogen ions from the solution.

Because of points (i)–(iii), measurements were also carried out discontinuously in this case. In addition, Na^+ concentration values below 0.04 ppm were not accounted for in the time lag analysis.

RESULTS AND DISCUSSION

Transport phenomena across membranes and related effects are well described in the literature (Refs. 16–20 and references cited therein). Nevertheless, it is useful to point out some basic concepts in order to better understand the approach followed in analyzing the experimental findings described in this article.

Theoretical Background

The most general model adopted to describe solute transport between the bulk of two solutions separated by a membrane is schematically shown in Figure 1. It is assumed that both sides of the membrane are covered by thin layers of immobile fluid of thickness δ, which depends on the fluidynamic conditions

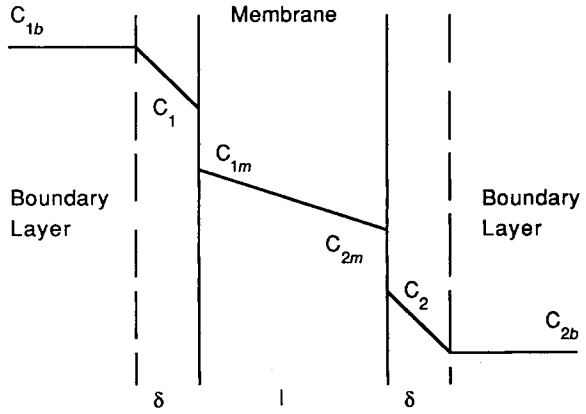

Figure 1 Schematic representation of the steady-state concentration profile across the membrane and the boundary layers; C_b and C_m are the solute concentrations in the bulk, and membrane phase, respectively; C is the solute concentration at the solution–membrane interface. Subscripts 1 and 2 refer to the feed and acceptor compartments, respectively.

operating in the bulk of the compartments. Solute transport from compartment 1 to compartment 2 consists of the following series of processes:

1. diffusion across the boundary layer via a diffusion mechanism with a solute diffusion coefficient equal to D_s;
2. sorption into the membrane;
3. diffusion across the membrane with a solute diffusion coefficient equal to D_m;
4. desorption out of the membrane; and
5. diffusion across the boundary layer.

Each step represents a resistance. Steps 1 and 5 are usually not rate determining as is the case in gas phase permeation. In addition, resistances due to steps 2 and 4 are lower than resistances due to step 3. Equilibrium is therefore generally assumed to be at the solution–membrane interfaces. For any species, we may thus write[16]

$$K_i = \frac{C_{im}}{C_i} = K_{0,i}K_{1,i} \tag{1}$$

where C_i and C_{im} are the solute concentrations in moles per unit volume of aqueous solution in the bath and in the membrane respectively; $K_{0,i}$ and $K_{1,i}$ are expressed by the following equations:

$$K_{0,i} = \frac{\gamma_i}{\gamma_{i,m}} \exp\left(\frac{-\Delta\mu_i^0 + \bar{V}_i\,\Delta P}{RT}\right) \tag{2}$$

$$K_{1,i} = \exp(-z_i F\Delta\phi/RT) \tag{3}$$

where γ_i and $\gamma_{i,m}$ are the activity coefficients, $\Delta\mu_i^0$ is the difference in standard chemical potential between the membrane and bath phase, $\bar{V}_i$ the molar volume of the ion, ΔP the swelling pressure, z_i the ionic charge, $\Delta\phi$ the potential difference, F the Faraday constant, R the gas constant, and T absolute temperature. Equations (1)–(3) describe ionic exclusion from the membrane by (i) differences in μ^0 and in the activity coefficients ($K_{0,i}$) and (ii) potential exclusion (Donnan effect) ($K_{1,i}$). Here $K_{0,i}$ is the only exclusion factor operating for neutral species or for ions in uncharged membranes.

The presence of the boundary layers will reduce the available driving force for diffusion inside the membrane. To account for these additional resistances to ionic transport, the simplest case of $\delta = 0$ is considered. Subsequently the real case $\delta \neq 0$ will be analyzed.

$\delta = 0$

In this case $C_{1b} = C_1$ and $C_{2b} = C_2$. If C_1 and C_2 are kept constant, a steady-state is reached in which the concentration remains constant at all points of the membrane and the flux J is given by

$$J = D_m \frac{C_{1m} - C_{2m}}{l} = D_m K \frac{C_1 - C_2}{l} \tag{4}$$

where the distribution coefficient K has been introduced and assumed constant with concentration. If the membrane thickness l and the surface concentrations C_1 and C_2 are known, the product $D_m K$ can be deduced from the measurements of J by using eq. (4). The product $D_m K$ is known as the *permeability coefficient* P. Its dimensions are centimeters squared per second. Thus, at steady state the measurable transport coefficient is the permeability P rather than the diffusion coefficient D_m.

Alternatively, both D_m and P can be obtained via unsteady-state measurements. In this case, the unsteady-state diffusion equation needs to be solved. In the scope of the present work, a useful relation is[21]

$$\frac{Q_t}{KSlC_{1b}} = \frac{D_m t}{l^2} - \frac{1}{6} - \frac{2}{\pi^2} - \frac{2}{\pi^2}\sum_1^\infty \frac{(-1)^n}{n^2} \exp\left(-\frac{D_m n^2 \pi^2 t}{l^2}\right) \tag{5}$$

where S is the membrane surface and Q_t is the total amount of substance emerging from the surface at $x = l$, i.e.,

$$Q_t = \int_0^t SD_m \left(\frac{\partial C}{\partial x}\right)_{x=l} dt \tag{5a}$$

Equation (5) can be applied when the membrane is initially at zero concentration and the face at $x = l$ is maintained effectively at zero concentration.[21]

As $t \to \infty$, Eq. (5) approaches the limit:

$$\frac{Q_t}{KSlC_{1b}} = \frac{D_m t}{l^2} - \frac{1}{6} \tag{6}$$

which, on a plot of Q_t versus t, has an intercept Θ on the t axis given by

$$\Theta = \frac{l^2}{6D_m} \tag{7}$$

Equations (6) and (7) have been used extensively as the basis of a method of obtaining the diffusion coefficient D_m from Eq. (7) and the permeability coefficient P from the slope of Eq. (6). Since $Q_t = C_{2b}V$ (where V is the volume of the acceptor compartment), by the knowledge of the transient $C_{2b}(t)$, P can be easily evaluated. In addition, the following requirements must be fulfilled: (i) $C_2(\approx 0) \ll C_1$ and (ii) Eq. (5) reduces to Eq. (6) when $D_m t/l^2 \geq 0.45$.

$\delta \neq 0$

The simplest case of diffusion for $\delta \neq 0$ is the one in which the membrane is in chemical equilibrium with its external bathing solutions, except that on the feed side a known amount of isotopically labeled solute is added. In this case the flux of labeled solute in the membrane is still described by Fick's law, where D_m now represents the tracer diffusion coefficient. The plot of the total radioactivity in the acceptor compartment has the same features as in the case of $\delta = 0$. In addition, due to the boundary layers at the membrane interfaces, isotopic concentrations measured in the bulk of both compartments differ from those at the membrane–solution interfaces. The permeability coefficient P cannot be deduced from Eq. (6). The steady-state regime is, in this case, described by the following equation:

$$J = D_s \frac{C_{1b} - C_1}{\delta} = D_m K \frac{C_1 - C_2}{l} = D_s \frac{C_2 - C_{2b}}{\delta} \tag{8}$$

Elimination of C_1 and C_2 yields

$$J = P_{exp} \frac{C_{1b} - C_{2b}}{l} \tag{9}$$

where the experimental permeability P_{exp} is given by

$$P_{exp} = \frac{D_m K}{1 + 2(D_m K\delta / D_s l)} \tag{9a}$$

Equation (9) has the form of Fick's law. The permeability coefficient that can be obtained by the steady-state part of the transient experiment via Eq. (9) is P_{exp}, not P. If $D_s l \gg D_m K\delta$ then $P_{exp} = P$. If $D_s l \ll D_m K\delta$, $P_{exp} = D_s$. In the former case the overall rate is controlled by the process across the membrane while in the latter the mass transport is under film diffusion control. Membrane control is favored by small D_m and/or small K (as in the case of Donnan exclusion), efficient stirring, and usage of thick membranes.

To obtain the true permeability P from the P_{exp} value, two methods have been used in the literature.[22-24] Rearranging Eq. (9a), one has

$$\frac{1}{P_{exp}} = \frac{1}{P} + \frac{2\delta}{D_s l} \tag{10}$$

where P can be obtained either (i) by performing a set of measurements with membranes of different thicknesses and plotting $1/P_{exp}$ versus $1/l$ (a linear extrapolation to $1/l = 0$ yields the true permeability P) or (ii) if the correlation between δ and the rate of stirring ω is known (usually of the form $\delta = A\omega^{-n}$) by plotting $1/P_{exp}$ versus ω^{-n}, which yields P as the value extrapolated at $\omega^{-n} = 0$.

When the experiment is conducted with two solutions of different concentration (as is usually done), a further effect must be taken into account. With this experimental configuration, i.e., high concentration in the feed compartment and distilled water in the acceptor compartment, solute flux occurs opposite to the solvent flux, which migrates from the dilute to the concentrated sides of the membrane. The solute flux in the membrane phase is, in this case, described by the equation

$$J = D_m \frac{\partial C}{\partial x} - C(1 - \sigma) P_w \Delta\pi \tag{11}$$

where σ is the Staverman reflection coefficient, P_w the membrane water permeability (in cm/s atm), and $\Delta\pi$ the osmotic pressure difference (in atm).[25] Usually, σ is closely related to the polymeric structure of the membrane. It varies between zero (grossly porous membranes) and 1 (very dense membranes). When solute transport occurs against solvent transport, Eq. (11) rather than Eq. (4) should be used.

The last part of this section is devoted to the introduction and to use of the "quasi-stationary-state" in membrane transport. If the volumes of both feed and acceptor compartments are so large that solute concentrations do not appreciably change with time, we may write

$$V \frac{\partial C_{2b}}{\partial t} = S P_{exp} \frac{C_{1b} - C_{2b}}{l} \tag{12}$$

After integration Eq. (12) yields

$$\ln(C_{1b} - C_{2b}) = -\frac{SP_{exp}}{Vl} t + \ln(C_{1b} - C_{2b})_0 \quad (13)$$

where the constant $\ln(C_{1b} - C_{2b})_0 \neq \ln C_{1b}$ [even if $C_{2b}(0) = 0$] is due to the quasi-steady-state approximation.

Equation (13) enables evaluation of P_{exp} by plotting $\ln(C_{1b} - C_{2b})$ versus t. The slope of this plot is proportional to P_{exp}, where P_{exp} is sometimes evaluated using Eq. (9) and assuming $C_{1b} - C_{2b} \approx C_{1b}$. In practice, this approximation is usually good, but inappropriate use may lead to underestimation of P_{exp}. The P_{exp} is determined by the equation

$$P_{exp} = \frac{Vl}{SC_{1b}} \frac{\partial C_{2b}}{\partial t} \quad (14)$$

where $\partial C_{2b}/\partial t$ is taken as the best linear least squares fit of the transient $C_{2b}(t)$ taking into account all the experimental data.[14] Equation (14) can be derived from Eq. (13) assuming (incorrectly) $\ln(C_{1b} - C_{2b})_0 = \ln C_{1b}$. This, as has already been pointed out, cannot be applied to the quasi-steady-state analysis because it leads to underestimated values of P_{exp}.

DISCUSSION

Recent work on ionic diffusion across PI indicates that hydrogen fluoride diffuses through PI as the associated species HF.[14] No ionic diffusion was detected for diffusants like KOH, NaOH, and HCl for experiments lasting 20 min or more. Assuming 20 min as the time lag and applying Eq. (7), we may estimate the order of magnitude of ionic diffusion coefficients, i.e., $D_m < 10^{-12}$ cm^2/s. On the basis of this estimate, long-run experiments were performed, as can be seen from the time scale of the experimental findings reported in Figures 2–5. With inspection of these figures, the time scale appears consistent with the data described in the preceding, i.e., times on the order of hours are necessary to measure appreciable concentration change in the acceptor compartment (a concentration of 1 ppm can only be detected after 10 h).

Figure 2 shows the Na^+ and the Cl^- concentrations in the acceptor compartment for a 2.4-μm-thick PMDA/ODA. The results for a Nafion membrane are shown for comparison. As can be seen,

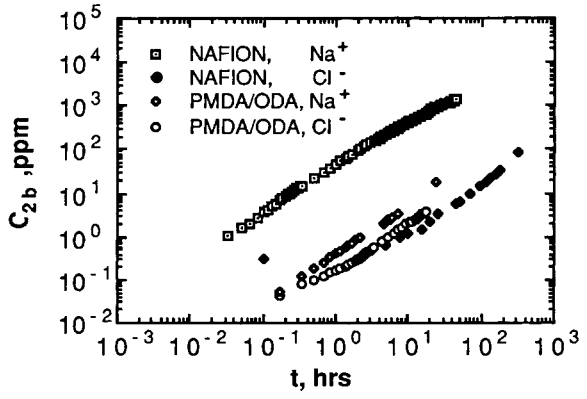

Figure 2 Ionic concentration in the bulk of the acceptor compartment as a function of time for Nafion and PMDA–ODA membranes (2.4 μm thick) at 30°C. Feed concentration was 5M NaCl.

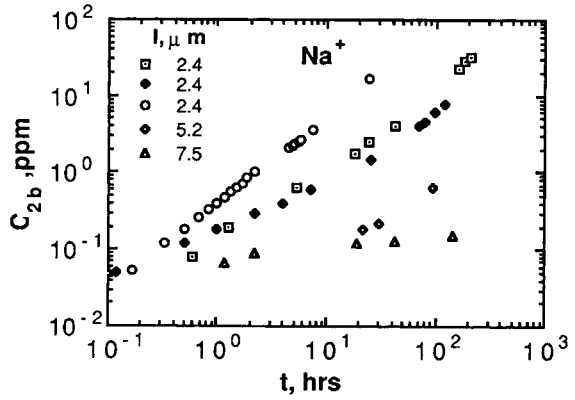

Figure 3 Na^+ ion concentration in the bulk of the acceptor compartment as a function of time for different samples of PMDA–ODA (2.4 μm) and Kapton films (7.5 μm). Temperature was 30°C and feed concentration 5M NaCl.

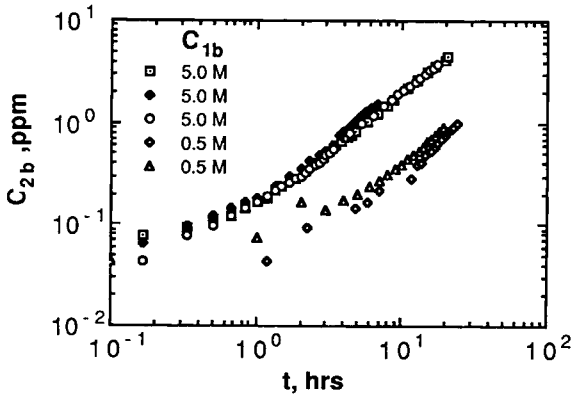

Figure 4 Cl^- ion concentration in the bulk of the acceptor compartment as a function of time for PMDA–ODA (2.4 μm thick) for different values of feed concentration. Repeated runs on the same sample are also reported. Temperature was 30°C.

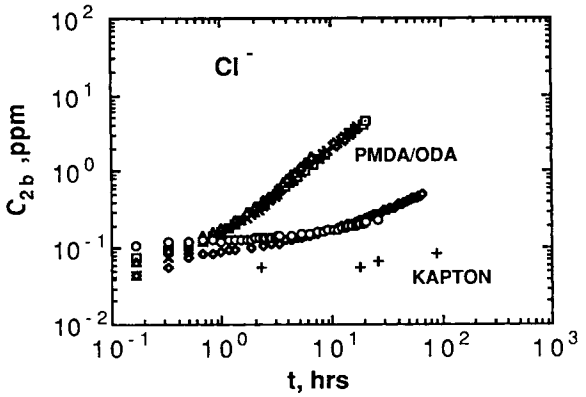

Figure 5 Observed scatter of chloride ion concentration in the bulk of the acceptor compartment as a function of time for PMDA–ODA (2.4 μm thick) at 30°C. Feed concentration was 5M NaCl.

Na^+ is easily transported across Nafion, whereas Cl^- permeability is comparable to that of Na^+ and Cl^- across PI. Nafion is a cationic exchange membrane, thus a Donnan exclusion mechanism is operating. This lowers the chloride content in the membrane phase, according to Eq. (3). In turn, this results in a lower permeability coefficient. The Cl^- and Na^+ diffusion coefficients in Nafion membranes are of the same order of magnitude. This is because ionic diffusion is much less affected by the fixed ionic groups of the polymeric matrix.

Results of Na^+ and Cl^- transport across PI reported in this figure also exhibit the same features as those exhibited by Nafion. The difference in sodium and chloride ion permeability can be ascribed to the negative fixed charge present in PI. Presence of unreacted polyamic acid has been reported in the literature for PI and Kapton.[8,26] However, the difference between sodium and chloride transport reported in Figure 2 are not likely due to a Donnan exclusion mechanism, as will be shown in the following.

In Figure 3 the effect of thickness on sodium transport for 2.4- and 5.2-μm-thick PI and for a 7.5-μm Kapton film is reported. In order to check reproducibility of the data and reliability of the film, many samples of the same thickness were tested. Results such as those reported in Figure 3 for Na^+ and in Figures 4 and 5 for Cl^- show that (i) reproducibility is excellent for repeated runs with the same sample (see Fig. 4), (ii) differences in the ionic permeabilities were found among membranes of the same thickness (see Figs. 3 and 5), and (iii) the lower the thickness, the broader the range of experimental findings (see Fig. 5). A quantitative analysis is described in the next section.

Flux Equation

A rough estimate of the ionic diffusion coefficient across PI can be attempted on the basis of the data recently reported.[14] Assuming a hypothetical time lag on the order of 20 min, Na^+ and Cl^- ions should diffuse across a 2.4-μm-thick film with a diffusion coefficient equal to 8×10^{-12} cm^2/s [see Eq. (7)]. Water transport in both PI and Kapton films is well documented in the literature.[6–10,27–29] Water sorption in PI is described either according to Henry's law or by a dual-mode sorption mechanism. Water transport is Fickian in nature, and a good estimate of its diffusion coefficient is 10^{-9} cm^2/s.[6–10,28] Even if we assume a salt diffusion coefficient on the order of 10^{-11} cm^2/s (which is certainly an underestimation), the ratio $(D_{H_2O}/D_s)_m \gg 1$. Under this circumstance, the coupling between water and salt flux is negligible, and for all practical purposes we may assume the Staverman's reflection coefficient $\sigma \approx 1$.[25] Thus, in this case, we may still apply Fick's law for ionic solute transport in the membrane phase. This result indicates that the experimental approach used in the literature[14] and here is equivalent to the use of labeled isotopic tracers.

Boundary Layer Estimation

It is useful to estimate in general form the order of magnitude of the group $(2D_mKS)/(D_sl)$ appearing in Eq. (9) to ascertain its importance in affecting the relationship between P_{exp} and P.

For all cases described in this article, the membrane thickness l is on the order of 10^{-3}–10^{-4} cm. An estimate of D_m has been reported in the preceding as $< 10^{-11}$ cm^2/s whereas $D_s \approx 10^{-5}$ cm^2/s. In forced convection and for geometries close to that of a diffusion cell, the widest range of δ reported is 10^{-2}–10^{-3} cm.[30,31] The value of K is open to the largest degree of uncertainty. A range of 10^{-2}–10 has been reported in the literature for several classes of polymers.[16,19,32] From the preceding values, it is found that $(2D_mKS)/(D_sl)$ ranges from 10^{-8} to 10^{-3}. Even by taking the maximum value of $(2D_mKS)/(D_sl)$, one finds that $(2D_mKS)/(D_sl)$ can be neglected with respect to 1 in the denominator of the expression of P_{exp} [Eq. (9a)]. The conclusion is drawn that the boundary layer does not affect ionic transport across PI. Boundary layers are ineffective even in the absence of stirring in the feed compartment, as recently described for HF diffusion [14]. Experimental results on the effect of stirring rate on Na^+ and Cl^- transport presented in this study are in agreement with the theoretical findings

described in the preceding and have been omitted for the sake of simplicity.

Time Lag Analysis

On the basis of the preceding conclusions, we may apply Eqs. (5)–(7) to the concentration transient in the acceptor compartment. Some results are reported in Figures 6 and 7. After a preliminary period of time necessary for the establishment of the steady-state, C_{2b} increases linearly with time. Extrapolating this linear part to the abscissa, the time lag Θ is derived, and hence the diffusion coefficient D_m can be computed by using Eq. (7). Since the slope of the linear part of this plot is equal to PSC_{1b}/lV [see Eq. (6)], the permeability P can easily be obtained. The distribution coefficient $K = P/D_m$ was also estimated. The full line reported in Figures 6 and 7 is the theoretical curve [Eq. (5)] and is in good agreement with the experimental findings.

As already mentioned, large discrepancies were observed among the samples tested. The widest observed range of P, D_m, and K for sodium and chloride transport across PI and Kapton are reported in Table I. In some cases, only estimates are reported due to the long time (10^3 h) required to establish the steady state across the film. As can be seen from Table I, the sodium diffusion coefficient varies between 1 and 13.3×10^{-13} cm^2/s for the thicknesses investigated. The estimate of the sodium diffusion coefficient across a 7.5-μm-thick Kapton film was $\approx 10^{-13}$ cm^2/s. Discrepancies among permeability coefficients were more pronounced with values ranging from 30×10^{-14} to 1.0×10^{-11} cm^2/s (two orders of magnitude). The estimate permeability for

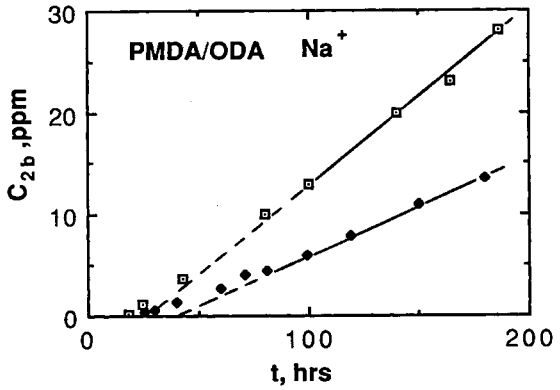

Figure 6 Time lag analysis for the establishment of steady state for the ionic transport of sodium across PMDA-ODA. Full and dotted lines represent Eqs. (5) and (6), respectively. Feed concentration was 5M NaCl; temperature, 30°C.

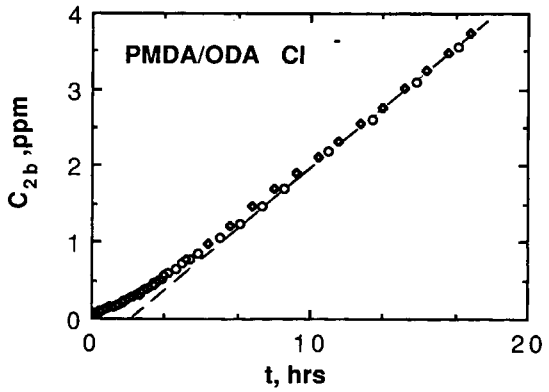

Figure 7 Time lag analysis for the establishment of steady-state for the chloride ion transport across PMDA–ODA. Full and dotted lines represent Eqs. (5) and (6), respectively. Feed concentration was 5M NaCl; temperature, 30°C.

Kapton film was even lower ($\approx 10^{-15}$ cm^2/s). Similar findings were obtained for Cl^- transport. For instance, Cl^- diffusion coefficients varied from 1.3×10^{-13} to 6.7×10^{-13} cm^2/s whereas the range of permeability values was 1.1×10^{-11}–8×10^{-14} cm^2/s. Estimates of diffusion and permeability coefficients across Kapton films were found to be very close to those reported in the preceding for Na^+.

The data reported in this article cannot be compared with literature data due to the few published ionic transport studies across PI. Paucity of Na^+ and Cl^- permeabilities, however, are such that no significant concentration changes can be observed for experiments lasting less than hours. This result is consistent with the HF diffusion data through PI for which 30 min was sufficient for establishing the steady-state. In addition, values of Na^+ permeabilities across Kapton $< 10^{-14}$ cm^2/s have been reported recently.[33] This is in the range reported here.

Although the observed discrepancies among otherwise similar membranes are not well understood, an attempt will be made to explain such anomalies as described in what follows.

Effect of Heterogeneities

The observed differences of the permeability values might be ascribed to defects like holes or thickness heterogeneities. It is useful to estimate the size of holes that may be present. From Figure 6, one has $\partial C_{2b}/\partial t \approx 1.4 \times 10^{-5}$ ppm/s. Since $V = 120$ cm^3, $l = 2.4 \times 10^{-4}$ cm, and $C_{1b} = 1 \times 10^5$ ppm, Eq. (15) yields $P_{exp}S \approx 4 \times 10^{-12}$ cm^4/s. If we attribute all the Cl^- transport to one hole, we find a defect on the order of 6 μm (assuming $P_{exp} \approx 10^{-5}$ cm^2/s),

Table I Observed Scatter Range of Na^+ and Cl^- Ionic Diffusion Coefficient D_m, Permeability Coefficient P, and Distribution Coefficient K for PMDA–ODA and Kapton Films at 30°C

Ion	l (μm)	C_{1b} (M)	$D_m \times 10^{13}$ (cm^2/s)	$P \times 10^{14}$ (cm^2/s)	K
			PMDA–ODA		
Cl^-	2.4	0.5	3.6–3.8	1000–1100	28–30
Cl^-	2.4	5	1.3–6.7	8–490	0.61–7.3
Na^+	2.4	5	1.0–13.3	180–1080	18–8
Na^+	5.2	5	1.3–1.4	30	2.3
			Kapton		
Cl^-	7.5	5	≈ 1[a]	≈ 0.1[a]	≈ 0.01[a]
Na^+	7.5	5	≈ 1[a]	≈ 0.1[a]	≈ 0.01[a]

[a] Estimated values.

which should be visible even under an optical microscope. SEM analysis carried out on different specimens showed the presence of relatively diffuse shallow heterogeneities on the order of 0.5 μm. No visible holes were detected. Since the stirring rate does not affect the transient, the presence of both holes and macroscopic defects can be excluded. Conversely, microscopic diffuse inhomogeneities might be present and could be responsible for the observed scattering.

The good agreement between the experimental results and the time lag analysis is remarkable (see Figs. 6 and 7). Thus, the observed discrepancies seem to be more physical in nature and not related to macroscopic defects. In the subsequent section, an attempt will be made to explain such discrepancies on the basis of water sorption mode and on the presence of contaminants.

Effect of Contaminants

Contaminants coming from the processing or from the blend supplied by the manufacturer could affect ionic permeabilities. The manufacturer estimates the sodium contamination level in PI to be 1 ppm. This is in agreement with literature data.[13] The presence of contaminants in the polymeric matrix can affect ionic transport in two ways: (i) the time lag data and (ii) they may act as a sink for the water dissolved in the membranes. In the former case, one has[20]

$$\Theta = \frac{l^2}{6D_m}\left[1 - 3\frac{KC_0}{C_{b1}}\right] \qquad (15)$$

where C_0 is the contaminant concentration in moles per cubic centimeter present in the PI. This effect could account for some discrepancies observed in the time lag experiments. However, C_0 does not play any role once the steady-state is reached.

The effect of water as a sink is more subtle. The equipotential volume model, EVM (see Chapter 5 of Ref. 16 and Chapter 10 of Ref. 19), will be used to describe this effect. According to this model, water in a polymeric matrix is separated in the "free" and "bound" solvent components. Ions sorbed by the membrane are considered to be dissolved in the imbibed water. The resulting "internal solution" is assumed to be normal aqueous solution in thermodynamic equilibrium with the external solution. This equilibrium is described by Eqs. (2) and (3). In addition, ions can diffuse only through the free water with a diffusion coefficient D_m given by

$$D_m = D_s\left(\frac{1 - V_p}{1 + V_p}\right)^2 \qquad (16)$$

where V_p is the volume fraction of the polymeric matrix.[34]

Water uptake in Kapton and in PI films is well documented in the literature.[6–9,27,28,35] Estimates of water content in the range of 2–5 g water/100 g dry polymer have been reported. Since the density of PI is 1.4 g/cm^3, the highest V_p is about 0.973 and the lowest ionic diffusion coefficient predicted by Eq. (16) is about 10^{-9} cm^2/s. This value is two to three orders of magnitude higher than the diffusion data reported in Table I. It can be concluded that the volume fraction through which ions may diffuse differs from that based on the water uptake. The amount of "bounded" water might well exceed that of free water. A rough estimate of the latter can be attempted by using the diffusion data reported in this work and Eq. (16). Carrying out this calcula-

tion, 0.1% as free water in PI is obtained. This value is only 5% of the total water uptake (assumed equal to 2% in the preceding analysis).

Sorption modes in PI have been described in the literature.[6-9] For a polymeric–penetrant couple, two forms of sorbed penetrant can be distinguished: a mobile (C_D) and an immobile (C_H) fraction. The C_D accounts for a sorption mechanism according to Henry's law whereas C_H accounts for a Langmuir-type sorption on internal pore surfaces at low activities and by clustering at higher activities. Water sorption in Kapton according to the former mechanism and to a more complex dual-mode sorption model (accounting for both C_D and C_H contributions) has recently been described in the literature.[6-9] The question of which sorption mode operates has a strong impact of the analysis of the findings reported in this article. If the first mechanism is operating, the water content could, in principle, be regarded as free water. Only a fraction of water would be free in the latter case. In addition, the effect of contaminants may also strongly decrease the volumetric fraction occupied by the free water due to the solvation process. The latter takes place between contaminants and water. An example of such an effect was described in the literature for 7.5 μm Kapton exposed to 75% RH.[36] Macroscopic increase of DC conductivity was attributed to the participation of the conduction process of *only* a fraction of ionic contaminants detected in the film. This is because ions are expected to be transported in a hydrated shell (at least Na^+). This process requires water aggregates large enough to hydrate ions. Of course, only free water is available for such a process. We may thus conclude that discrepancies of ionic permeabilities may be ascribed to both contaminants and to water sorption modes. No macroscopic variations have been reported in the permeabilities of neutral molecules like HF across PI of different thicknesses.[14] This is in agreement with the preceding arguments. No experimental supporting evidence for this hypothesis can be presented because samples were too thin to carry sorption measurements. In addition, contamination due to Na^+ and Cl^- would have affected the determination of contaminant content. "*A priori*" defects such as "invisible holes," thickness inhomogeneities, and microcracks (developed by prolonged exposition to high concentration of NaCl[7]) may therefore not be excluded.

CONCLUSION

PMPA–ODA and Kapton PI membranes were found to be permeable to both Na^+ and Cl^-. Large variations in permeabilities were observed and tentatively ascribed to (i) heterogeneities such as invisible holes and (ii) both contaminants and free water content. Shallow defects on the order of 0.5 μm were detected by SEM. No experimental results were presented to support item (ii). Diffusion of neutral molecules across PI recently described[14] is consistent with the hypothesis described here because neither free water nor contaminants may strongly affect their permeation rate.

Results reported in this article are important to assess the reliability of PI as an organic packaging material in microelectronics. Due to the large water and oxygen permeabilities exhibited by PI,[6-12] corrosion of electronic circuitry in hostile environments is expected to be under ionic resistance control. Thus, large discrepancies could be expected when PMDA–ODA films 1–5 μm thick are used to protect metallic circuitry from corrosion.

Financial support from General Motors and the Shell Companies Foundation is gratefully acknowledged.

REFERENCES

1. J. D. Sinclair, *J. Electrochem. Soc.*, **135,** 89C (1988).
2. P. Milner in *Agenda for Advances in Electrochemical Corrosion Science and Technology,* publication NMAB 438-2, National Academy Press, Washington, D.C., 1987, p. 67.
3. A. M. Wilson, *Thin Solid Films,* **83,** 145 (1981).
4. B. Comizzoli, R. P. Frankenthal, P. C. Milner, and J. D. Sinclair, *Science,* **234,** 340 (1987).
5. D. W. Cooper, *Aerosol Sci. Tech.*, **5,** 287 (1986).
6. E. Sacher and J. R. Susko, *J. Appl. Polym. Sci.*, **23,** 2355 (1979).
7. E. Sacher and J. R. Susko, *J. Appl. Polym. Sci.*, **26,** 679 (1981).
8. D. K. Yang, W. J. Koros, H. B. Hopfenberg, and V. T. Stannett, *J. Appl. Polym. Sci.*, **30,** 1035 (1985).
9. D. K. Yang, W. J. Koros, H. B. Hopfenberg, and V. T. Stannett, *J. Appl. Polym. Sci.*, **31,** 1619 (1986).
10. G. F. Sykes and A. K. St. Clair, *J. Appl. Poly. Sci.*, **32,** 3725 (1986).
11. R. M. Felder, C. J. Patton, and W. J. Koros, *J. Polym. Sci., Polym. Phys. Ed.*, **19,** 1995 (1981).
12. W. J. Koros, J. Wang, and R. M. Felder, *J. Appl. Polym. Sci.*, **26,** 2805 (1981).
13. H. J. Neuhaus, D. R. Day, and S. D. Senturia, *J. Elec. Mat.*, **14,** 379 (1985).
14. L. M. Doane, J. A. Bruce, and R. G. Narechania, *J. Electrochem. Soc.*, **135,** 3155 (1988).
15. M. Allen, M. Mehregany, R. T. Howe, and S. D. Senturia, *Appl. Phys. Lett.*, **51**(4), 241 (1987).

16. F. Helfferich, *Ion Exchange,* McGraw-Hill, New York, 1962.
17. S. B. Tuwiner, *Diffusion and Membrane Technology,* Reinhold, New York, 1962.
18. N. Lakshminarayanaiah, *Chem. Rev.,* **65,** 491 (1965).
19. J. Crank and G. S. Park, *Diffusion in Polymers,* Academic Press, New York, 1954.
20. W. Jost, Diffusion in Solids, Liquids, and Gases, Academic Press, New York, 1960.
21. J. Crank, *The Mathematics of Diffusion,* University Press, Oxford, 1968.
22. F. Bellucci, L. Nicodemo, A. Morcone, and T. Monetta, *J. Membr. Sci.,* **52,** 393 (1990).
23. D. G. Tsimboukis and J. H. Petropoulos, *J.C.S. Faraday I,* **75,** 717 (1979).
24. K. Tojo, Y. Sun, M. M. Ghannam, and Y. W. Chien, *AIChe J.,* **31,** 741 (1985).
25. O. Kedem, and A. Katchalsky, *Biochim. Biophys. Acta* **27,** 229 (1958).
26. P. D. Deck, and H. Leidheiser Jr., *Abstract 211,* The Electrochem. Society Extended Abstracts, Chicago, Illinois Oct. 9–14 (1988).
27. D. P. Malladi, J. R. Scherer, S. Kint, and G. F. Bailey, *J. Membr. Sci.,* **19,** 209 (1984).
28. D. D. Denton, D. R. Day, D. F. Priore, and S. D. Senturia, *J. Elec. Mat.,* **14**(2), 119 (1985).
29. F. Bellucci and R. M. Latanision, unpublished results.
30. T. G. Kaufmann and E. F. Leonard, *AIChE J.,* **14,** 421 (1968).
31. R. B. Bird, W. E. Stewart, and E. N. Lightfoot, *Transport Phenomena,* Wiley Int. Ed., New York, 1960.
32. B. Demetrios, G. Tsimboukis, and H. Petropoulos, *J.C.S. Faraday I,* **75,** 705 (1979).
33. B. Comizzoli, private communication.
34. J. S. Mackie and P. Meares, *Proc. Roy. Soc. (London) Ser. A,* 232, 485, 498, and 510 (1955).
35. G. Samuelson and S. Lytle, in *Polyimides: Synthesis, Characterization and Applications,* K. L. Mittal, Ed., Plenum Press, New York, 1984, vol. 2, p. 751.
36. E. Sacher, *IEEE Trans. Electr. Ins.,* **E1-14,** 85 (1979).

Received April 6, 1989
Accepted July 2, 1990